Numerical Solution of Differential Equations - Project 1

Sæther, Trym[1] and Haugen, Tor Ludvig Løvold[1]

[1]Department of Mathematical Sciences, NTNU

February 28, 2025

Abstract

We develop and analyze a reaction-diffusion SIR model on a 2D domain, coupling an explicit reaction update with a Crank–Nicolson approach for diffusion. The method is unconditionally stable in the linearized case and second-order accurate when time and space steps scale appropriately. Numerical tests illustrate infection spread patterns under varied initial conditions and spatially/time-dependent infection rates, highlighting both the scheme's stability and the simplifying assumptions that limit real-world applicability.

Contents

1 Introduction

Mathematical models are essential for the modern world to function. They are tools that modern society could not exist without. Specifically numerical models allow us to simulate a multitude of different scenerios, giving us insights into the mechanics of our world. One example of this is disease modeling. Accurate modeling of infectious disease spread requires capturing both the dynamics of transmission and how that transmission propagates across space. While the classical Susceptible Infected Removed (SIR) model offers insight into temporal evolution, it does not account for spatial movement of the population. To address this limitation, we extend the SIR framework to a reaction–diffusion system, adding diffusion terms that approximate individual mobility within a two-dimensional domain.

Such a PDE-based approach, however, raises numerical challenges: the diffusion and reaction components interact in ways that can destabilize straightforward explicit methods. To overcome this, we employ a finite difference method (FDM) in space combined with a modified Crank–Nicolson scheme in time that handles the diffusion term implicitly and the reaction term explicitly.

This report focuses on the theoretical underpinnings of this approach, assessing consistency and stability through classical analyses, then validates the method numerically. By exploring varying initial distributions of infection, different parameter regimes, and dynamic infection rates, we illustrate how the method captures key spatiotemporal patterns in disease spread while preserving computational efficiency and stability.

This report applies a finite difference method (FDM) for spatial discretization and a modified Crank–Nicolson scheme for time integration, treating diffusion implicitly and reaction explicitly. The objectives are to analyze the scheme's numerical properties, validate it through numerical experiments, and investigate disease spread under varying initial conditions and parameter settings.

2 Theory: Reaction–Diffusion Equation and Finite Difference Method's

2.1 Overview of the Numerical Method

We consider the reaction-diffusion equation

$$u_t \;=\; \mu\, u_{xx} \;+\; f(u), \quad x \in (0, L), \quad t > 0,$$

where $\mu > 0$ is the diffusion coefficient and $f(u)$ is a reaction term. We discretize space by dividing $(0, L)$ into $M + 1$ subintervals of uniform width $h = L/(M + 1)$, so the grid points are $x_m = m\, h$ for $m = 0, \ldots, M + 1$. In time, we use a step $k > 0$, so $t_n = n\, k$. Let $U_m^n \approx u(x_m, t_n)$. Then we define the dimensionless parameter

$$r \;=\; \frac{\mu\, k}{h^2}.$$

The scheme combines a Crank–Nicolson-like step for the diffusion term with an explicit component for the reaction. It approximates the spatial derivative at the midpoint between time steps. It is unconditionally stable and second–order accurate in time and space. Concretely, each time–step consists of:

1. *Predictor*: approximate the diffusion term in a semi–implicit manner and add an explicit

reaction increment:

$$U_m^\star = U_m^n + \frac{r}{2}\left(\delta_x^2 U_m^\star + \delta_x^2 U_m^n\right) + k\, f\left(U_m^n\right)$$
$$\delta_x^2 U_m^n = U_{m+1}^n - 2\, U_m^n + U_{m-1}^n \qquad \text{(Central Difference Method)}$$

2. *Corrector*: apply a midpoint update for the reaction:

$$U_m^{n+1} \;=\; U_m^\star \;+\; \frac{k}{2}\Big(f\left(U_m^\star\right) - f\left(U_m^n\right)\Big).$$

Visually the scheme can be illustrated with a stencil as shown below. Clearly showing the discretization of the domain and how this is used to calculate the next value in time with the diffusion term calculated semi–implicitly and the reaction term explicity.

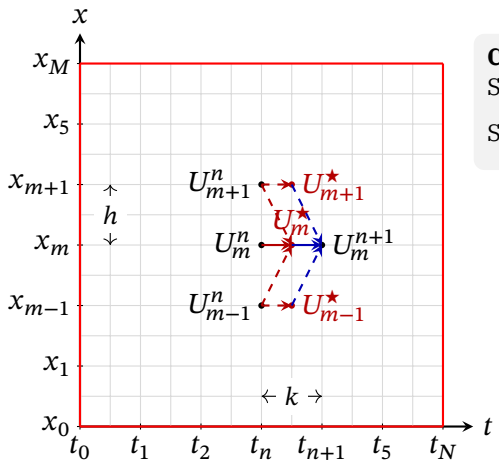

Crank–Nicolson:
Step 1 (Predictor): $U_m^* = U_m^n + \frac{r}{2}(\delta_x^2 U_m^* + \delta_x^2 U_m^n) + k f(U_m^n)$
Step 2 (Corrector): $U_m^{n+1} = U_m^* + \frac{k}{2}(f(U_m^*) - f(U_m^n))$

For the boundary conditions, either Dirichlet, Neumann, or Robin, one sets or solves for the boundary values U_0^n, U_{M+1}^n at each step as usual.

2.2 Error Analysis

To analyze the correctness of the scheme it is neccessary to determine both the consistency and stability of the scheme. This is because a numerical method converges if, and only if, it is both consistent and stable.

2.2.1 Consistency

Consistency ensures that as the discrete step sizes approach zero, the numerical scheme's approximation converges to the original differential equation. In other words, consistency guarantees that we are actually solving the intended continuous problem rather than some other unrelated equation. To determine the consistency of the modified Crank–Nicolson scheme for the PDE with the linear reaction term $f(u) = au$, we analyze the local truncation error (LTE) by substituting the exact solution into our numerical scheme.

Theorem 1. Local truncation error for the modified Crank–Nicolson

For the PDE $u_t = \mu u_{xx} + au$ with constant a, the modified Crank–Nicolson scheme with steps h (space) and k (time) has local truncation error

$$\|\tau_m^n\| = \mathcal{O}\left(k + \frac{h^4}{k}\right)$$

where $u_m^n = u(x_m, t_n)$ is the exact solution and U_m^n its numerical approximation. Under parabolic scaling $k \propto h^2$, the scheme achieves second-order accuracy:

$$\|\tau_m^n\| = \mathcal{O}\left(h^2 + k^2\right)$$

Proof of Theorem 1. We analyze the truncation error by examining how the exact solution satisfies the numerical scheme. First, consider (Central Difference Method) for the second spatial derivative:

$$\delta_x^2 u_m^n = h^2 u_{xx}(x_m, t_n) + \mathcal{O}(h^4)$$
$$\delta_x^2 u_m^\star = h^2 u_{xx}(x_m, t_n) + \mathcal{O}(h^4 + k^4)$$

Step 1 (Predictor): Substituting the exact solution into the first stage:

$$u_m^\star = u_m^n + \frac{r}{2}\left(\delta_x^2 u_m^\star + \delta_x^2 u_m^n\right) + kau_m^n = u_m^n + \frac{\mu k}{2} u_{xx}(x_m, t_n) + kau_m^n + \mathcal{O}(h^4 + k^4)$$

Step 2 (Corrector): For the second stage:

$$u_m^{n+1} = u_m^\star + \frac{k}{2}(au_m^\star - au_m^n)$$

From the PDE, we know $u_t = \mu u_{xx} + au$ and can derive expressions for higher time derivatives. Using Taylor expansion:

$$u(x_m, t_n + k) = u_m^n + ku_t + \frac{k^2}{2} u_{tt} + \frac{k^3}{6} u_{ttt} + \mathcal{O}(k^4)$$

Comparing this with our numerical solution, we obtain:

$$U_m^{n+1} - u_m^{n+1} = \mathcal{O}(k^2 + h^4)$$

The local truncation error per step is thus:

$$\|\tau_m^{n+1}\| = \frac{|U_m^{n+1} - u_m^{n+1}|}{k} = \mathcal{O}\left(k + \frac{h^4}{k}\right)$$

Under the parabolic scaling $k \sim h^2$, we have $\frac{h^4}{k} \sim h^2$, yielding second-order accuracy:

$$\|\tau_m^{n+1}\| = \mathcal{O}(h^2 + k^2)$$

□

2.2.2 Stability Analysis

Stability ensures errors do not grow uncontrollably. Without both, one cannot guarantee convergence. We investigate whether the scheme can tolerate large time steps without amplification of numerical errors, thus satisfing the conditions for stability. For linear problems $u_t = \mu\, u_{xx} + a\, u$, a von Neumann analysis is done to see whether this is true.

Theorem 2. von Neumann Stability for modified Crank–Nicolson

The modified Crank–Nicolson scheme for the PDE with a linear reaction term $f(u) = au$ is unconditionally stable for any choice of step sizes h and k, as the amplification factor ξ satisfies:

$$|\xi| \leq 1 + Ck$$

for some constant C independent of step sizes.

Proof of Theorem 2.
We apply von Neumann stability analysis by studying how individual Fourier modes $U_m^n = \xi^n e^{i\beta mh}$ evolve under our scheme, where β is the wave number. As previously statet the PDE with a linear reaction term $f(u) = au$, the two-stage modified Crank–Nicolson scheme is given by:

$$U_m^\star = U_m^n + \frac{r}{2}\left(U_{m+1}^\star - 2U_m^\star + U_{m-1}^\star + U_{m+1}^n - 2U_m^n + U_{m-1}^n\right) + kaU_m^n$$
$$U_m^{n+1} = U_m^\star + \frac{ka}{2}(U_m^\star - U_m^n)$$

Substituting the Fourier modes $U_m^n = \xi^n e^{i\beta mh}$ and $U_m^\star = \xi^n \xi^\star e^{i\beta mh}$

$$\xi^\star = \frac{1 - r\sin^2(\beta h/2) + ka}{1 + 2r\sin^2(\beta h/2)}, \quad \text{where} \quad s = \sin^2(\beta h/2)$$

For the second stage:

$$\xi^{n+1} = \xi^n \left[\xi_\star\left(1 + \frac{ka}{2}\right) - \frac{ka}{2}\right]$$

Therefore, the amplification factor is:

$$\xi = \frac{\left(1 - r\sin^2(\beta h/2) + ka\right)\left(1 + \frac{ka}{2}\right) - \frac{ka}{2}\left(1 + 2r\sin^2(\beta h/2)\right)}{1 + 2r\sin^2(\beta h/2)}$$

After algebraic simplification, and substituting $s = \sin^2(\beta h/2)$:

$$\xi = \frac{1 - rs(1 + \frac{3}{2}ka) + ka + \frac{1}{2}k^2a^2}{1 + 2rs}$$

Then for $a \geq 0$ and any $r > 0$, both numerator and denominator are positive with $\xi(s) < 1$ for all $s \in [0, 1]$.
For $a < 0$, the worst case occurs at $s = 0$, giving:

$$\xi(0) = 1 + ka + \frac{k^2a^2}{2} = 1 + ka\left(1 + \frac{ka}{2}\right)$$

For sufficiently small k:

$$|\xi(0)| \leq 1 + |a|k(1 + |a|k/2)$$

Therefore, $|\xi| \leq 1 + Ck$ with $C = |a|(1 + |a|k/2) \approx |a|$ for small k, confirming the scheme is unconditionally stable. □

2.2.3 Global Error and Convergence

Theorem 3. Lax Equivalence and Convergence of Crank–Nicolson

Since the modified Crank–Nicolson scheme is both consistent and stable, by the Lax Equivalence Theorem it is convergent. Under the parabolic scaling $k \sim h^2$, the scheme achieves second-order convergence. Thus the global error satisfies:

$$\|e_m^n\| = \mathcal{O}(h^2 + k^2)$$

Remark 1

The proof follows directly from the Lax Equivalence Theorem, which states that for linear problems, if a numerical scheme is consistent and stable, it converges to the exact solution.

2.3 Numerical Verification

We verify the theoretical results by performing a convergence analysis of the modified Crank–Nicolson scheme for the reaction-diffusion equation with a linear reaction term. The numerical solution is compared to the exact solution, and the error is computed for different grid sizes. The results are shown in Figure 1. The parameters are set to $\mu = 1, L = 1, a = 1$, and the initial condition is given by $u(x, 0) = \sin(\pi x)$.

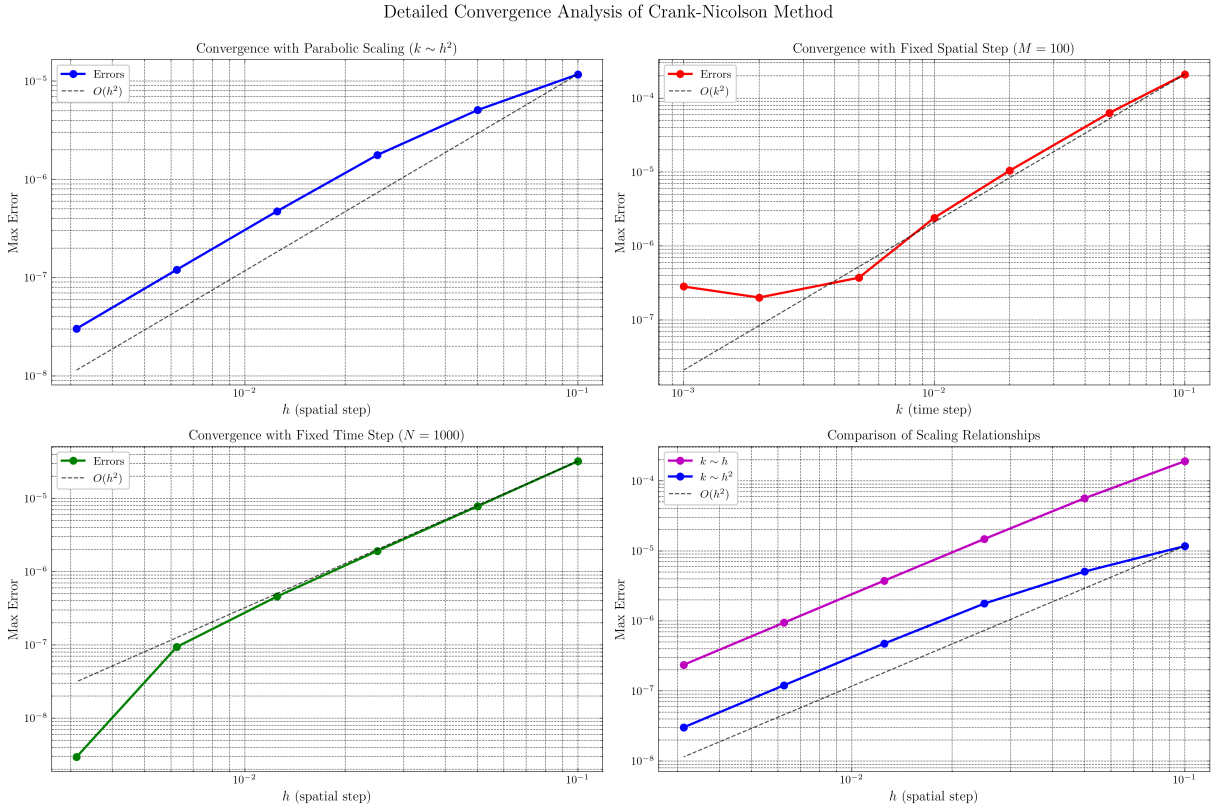

Figure 1: Convergence analysis of the modified Crank–Nicolson scheme for the reaction–diffusion equation with a linear reaction term.

The figure shows the convergence of the numerical solution to the exact solution as the grid is refined. The error decreases quadratically with respect to both h and k, confirming the second-order accuracy of the scheme. We can also confirm that choosing a parabolic scaling $k \propto h^2$ yields a better second-order convergence.

3 Application: Spatial-Temporal SIR Model

We study the spatial–temporal spread of a disease by extending the classic SIR model to two spatial dimensions. This results in a reaction–diffusion system for (S, I) on a square domain $\Omega = [0, L] \times [0, L]$. As discussed in the theory section this is a good candidate for the modified Crank–Nicolson scheme.

3.1 Model Formulation and Modifications

A classical SIR system tracks susceptible S, infected I, and removed R. At a single location, one has

$$\begin{cases} S'(t) &= -\beta\, S(t)\, I(t), \\ I'(t) &= \beta\, S(t)\, I(t) \;-\; \gamma\, I(t), \\ R'(t) &= \gamma\, I(t). \end{cases}$$

Here β is the infection rate and γ the recovery rate. And $S + I + R = 1$ when normalized to a unit population.

To allow disease to spread across a region, we introduce diffusion of S and I.

$$\begin{cases} S_t &= -\beta\, S I \;+\; \mu_S\, \Delta S, \\ I_t &= \beta\, S I \;-\; \gamma\, I \;+\; \mu_I\, \Delta I, \end{cases} \qquad (x, y) \in \Omega,\ t > 0.$$

We set $R = 1 - S - I$ and update it via $R_t = \gamma\, I$. Here $\Delta = \partial_x^2 + \partial_y^2$ is the 2D Laplacian, and μ_S, μ_I are diffusion coefficients.

Additionally to let this modell be better applicable to realistic scenarios we modify β to be dynamic in space and time, i.e. $\beta = \beta(x, y, t)$. Physically, it might be higher in densely populated areas or vary over time for example periodic public gatherings.

3.2 Numerical Implementation

3.2.1 Discretization of the Domain

We subdivide $\Omega = [0, L] \times [0, L]$ into an$M \times M$ grid. Let $h = L/M$ so that the grid points in each direction are $x_i = i\, h$, for $i = 0, \dots, M$. Combining, $\{(x_i, y_j)\}$ yields M^2 internal variables for each unknown (S and I). We use a unit square $(0, 1) \times (0, 1)$ with a 50×50 mesh for a compromise between resolution and runtime. A larger mesh would capture finer diffusion details but slow the simulation significantly.

We approximate $\Delta u \approx \partial_x^2 u + \partial_y^2 u$ by standard central differences. In one dimension (size M), the matrix for second differences is tridiagonal:

$$L_{1\mathrm{D}} = \mathrm{tridiag}\{1, -2, 1\} \in \mathbb{R}^{M \times M}$$

To handle a 2D Laplacian, we form $L_{2D} = \text{kron}(I, L_{1D}) + \text{kron}(L_{1D}, I)$, where kron is the Kronecker product and I is the $M \times M$ identity. This yields an $(M^2) \times (M^2)$ sparse matrix. In the code, laplacian() returns precisely this matrix.

3.2.2 Chosen Boundary Conditions and Parameters

A no-flux boundary condition is chosen, effectively, $\mu \Delta u$ is discretized so that outward flux is zero at the domain edges. This is reflected by the modified diagonal entries for the topmost and bottommost rows in L_{1D}. This is typical of a homogeneous Neumann implementation in central differences.A Neumann approach ensures people cannot exit or enter the domain, consistent with a self-contained population.

In the code, $\beta = 3$ and $\gamma = 1$ are chosen as baseline infection and recovery rates, matching simpler 1D SIR examples. We set μ_S and μ_I to small values so that susceptible and infected individuals do not diffuse too quickly. The domain is $L = 1$, and we choose $M = 50$, 50 intervals in each dimension, and a small time-step dt $= 0.001$ so that the PDE solution remains stable for the chosen parameters.

For the initial conditions there are three modes of "infected" initialization:

- `n=0`: Dense local infection in corners, using a Gaussian peak near $\frac{L}{4}, \frac{L}{4}$ plus its mirror.
- `n=1`: A linear front of infection occupying the leftmost 20% of the domain.
- `n=2`: Several random patches within the interior, mimicking local clusters.

We let $S = 1 - I$ initially (with $R = 0$). The choice of ≈ 0.01 sets how large the initial infection fraction is. The three distinct initial distributions show how infection geometry affects overall spread.

3.2.3 Beta function

As previously stated, the SIR model is modified when a dynamic beta, meaning that beta is a function dependent on both time and space. This is implemented via:

$$\beta(x, y, t) \;=\; \beta_0 \times \left[1 + 0.5\, e^{-100\,((x-\frac{L}{2})^2 + (y-\frac{L}{2})^2)}\right] \times \left[1 + 0.1 \sin(t - 2)\right] \quad (\text{for } 2 \le t \le 2 + \pi),$$

and equals the constant β_0 otherwise. The optional `dynamic_beta` toggles a time and space dependent infection rate to model gatherings.

3.2.4 Time-Stepping

Given $\Delta t = \text{dt}$,

$$S^{n+1} \;=\; S^n + \Delta t \left[\mu_S\, L_{2D}\, S^n - \beta(x, y, t_n)\, S^n\, I^n\right], \quad I^{n+1} \;=\; I^n + \Delta t \Big[\mu_I\, L_{2D}\, I^n + \beta\, S^n\, I^n - \gamma\, I^n\Big].$$

We also update $R^{n+1} = R^n + \Delta t \left[\gamma\, I^n\right]$. If β is dynamic, we compute $\beta(x, y, t)$ each step before forming the infection source term.

4 Experiments and Results

We simulate a two-dimensional SIR model with diffusion on a square domain $\Omega = [0, L] \times [0, L]$ using a 50×50 grid. The diffusion coefficients are set to $\mu_S = 0.001$ and $\mu_I = 0.001$, while the

infection rate $\beta = 3.0$ is modified to be spatially and temporally dependent, as described in the previous section.

The initial conditions are chosen at random, with random positions for the infected individuals, and the simulation runs for $T = 15$. At time $t = 8$, we introduce an event that increases the infection rate in the top half of the domain within a specific radius.

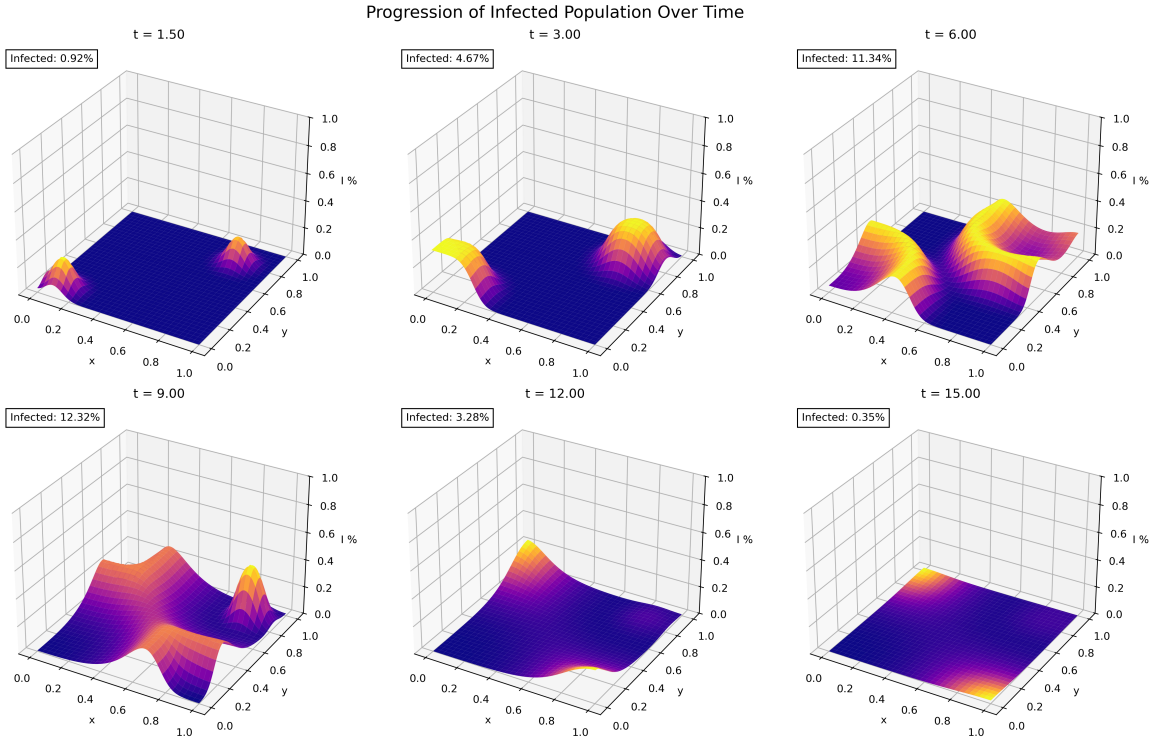

Figure 2: Progression of infected population over time.

We can see that the infected population increases rapidly from the initial conditions, and the event at $t = 8$ causes a significant local increase in the infected population. The event is not strong enough to cause a global increase in the infected population, as most of the population has already recovered and the infection rate is still decreasing. The event does, however, cause a local increase in the infected population, as can be seen in the figure.

5 Discussion

5.1 Theory versus Numerical Results

In principle, the linear stability analysis applies most directly if $f(u)$ is linear. Our tests used a strongly nonlinear infection term βSI, so the unconditional stability partially hinges on the moderate size of β and small time steps in practice. The local truncation argument still informs us that spatial errors scale like h^2 and temporal errors like k^2. Numerically, we see outcomes consistent with that prediction, but if one pushed the ratio k/h^2 too high or introduced extremely large β, the scheme could exhibit instability or large phase errors. Thus, while the theoretical $\mathcal{O}(h^2)$ accuracy remains a useful guideline, the real PDE problem is more delicate than a purely linear analysis

suggests.

5.2 Limitations of Numerical Scheme

Although our numerical scheme is supported by a consistency and stability analysis for linearized problems, it faces some caveats. First, the reaction-diffusion equation with a fully nonlinear reaction $f(u)$ may require additional care, especially if the reaction term grows quickly or exhibits stiff behavior. In that case, even though the scheme remains conditionally consistent, larger time steps may trigger inaccuracies in the reaction component.

5.3 Limitations of SIR Model

On the modeling side, our SIR setup simplifies many real-world complexities. The population is mostly uniformly distributed except for the small adjustments in $\beta(x, y, t)$, travel into/out of the region is ignored, and we do not address other realistic processes. While these simplifications permit tractable PDE computations, it means our conclusions about how infection waves propagate may not translate directly to real world situations

6 Conclusion

We presented a reaction-diffusion SIR model and applied a two-stage Crank–Nicolson-type scheme for the diffusion component, combined with an explicit update of the reaction term. The theoretical analysis confirmed that, the method achieves second-order local accuracy and is unconditionally stable for the linearized case. Numerical experiments with varying initial infections and dynamic infection rates demonstrated that the scheme captures essential features of spatiotemporal epidemics, such as localized outbreaks expanding over time. While our verification was primarily qualitative and relies on several simplifying assumptions the results shown that this approach provides a framework for modeling disease spread. Showing the importance and usefullness of numerical schemes for solving differential equations.